Research Article

A GA-based adaptive mechanism for sensorless vector control of induction motor drives for urban electric vehicles

Asma BOULMANE[1,*] , **Youssef ZIDANI**[1] , **Driss BELKHAYAT**[1], **Marouane BOUCHOUIRBAT**[2]
[1]Electrical Systems and Telecommunications Laboratory, Faculty of Science and Technology,
CADI AYYAD University, Marrakesh, Morocco
[2]High Institute of Engineering and Business (ISGA), Marrakesh, Morocco

Abstract: Induction motors are more attractive to car manufacturers because they are more robust and more cost effective to maintain in comparison with other types of electric machines. The evolution of their control makes them more efficient and less expensive. However, a new control technique known as sensorless control is being used to simplify the implementation of electric machines in electric vehicles. This technique involves replacing the flux and speed sensors with an observer. The estimation of these elements is based on the measurement of currents and voltages. The main purpose of the present study is to design a novel robust structure of the sensorless vector control for an urban electric vehicle. The proposed structure aims to improve the accuracy of dynamics at low speeds, eliminate sensitivity to the machine's parameters, and maintain the stability of the system even if the variation reaches high values. The speed estimation is ensured by an enhanced PI adaptation mechanism based on the full order Luenberger observer. The proof of this stability is based on the Lyapunov theorem. Moreover, a GA-based adaptive control is used for self-tuning of the stator resistance. By combining these techniques, we can enhance the efficiency and stability of the whole system.

Key words: Electric vehicle, induction machine, sensorless control, vector control, genetic algorithm, Lyapunov theorem, Luenberger observer

1. Introduction

Several factors have contributed to the major evolution of induction motor (IM) drives in recent decades: the availability and low cost of power inverters resulting from advances in power electronic switching devices and microprocessor-based controls, and the cost and availability of other sources of energy. Furthermore, the diversity and the mastery of electric motors, as well as the ease of controlling their torque over a range of speeds, have led car manufacturers to use them in the field of automotive traction [1].

Note that IMs are becoming the most widely used and the best choice for high power and variable speed applications because they have the best compromise of power density and manufacturing cost. IMs are simple in structure, robust and reliable, and require little maintenance [2]. Further, they can be designed with totally enclosed rotors to operate in dirty and explosive environments. These features make IMs attractive for use in industrial drives, especially automotive traction. Indeed, in automotive traction, whether the engine is thermal, hybrid, or electric, the desire is to have fast acceleration at low speed and operation over a wide range of speeds. For speeds above the basic speed, the drive can be used at constant power up to a maximum value-field weakening.

---

*Correspondence: asma.boulmane@gmail.com

The choice of electric motor is key to the performance of an electric vehicle. As described in Figure 1, the traction power of the wheels is delivered by the three-phase electric machine. The torque and speed of the machine are controlled by the voltage source inverter, which converts the battery DC voltage to a three-phase AC voltage suitable for the electric machine. A bidirectional DC–DC converter ensures a bidirectional energy transfer, which allows the battery to be charged during the braking phase.
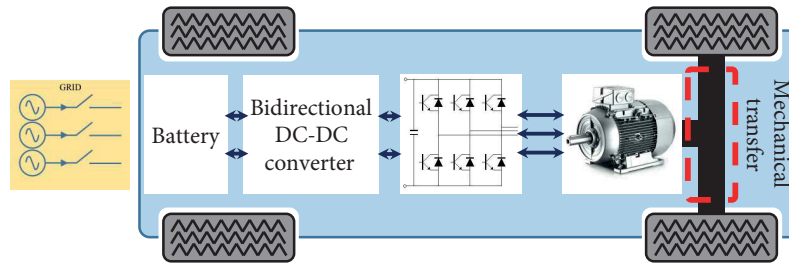

Figure 1. Electric vehicle architecture.

The control of these engines requires using a sensor to measure the speed (or position). This sensor increases the complexity, size, and price of the hardware needed for the system and brings several other disadvantages, including lack of reliability and noise immunity. The use of a sensorless control will increase the robustness and decrease the maintenance of the drive system [3, 4]. The idea is to replace the physical sensor with a software sensor. Thus, several techniques are used to accurately determine speed. Two main categories are developed in the literature [5–14]: a category that does not require knowledge of the motor model (signal injection) and the others based on the motor model.

The signal injection technique has many advantages, in particular stability and suitable response at low speed. Nevertheless, the choice of injected signal frequency becomes hard due to the difficulty of extracting correct information about the rotor position. However, this technique is rarely used in induction machine drive applications. The model reference adaptive system (MRAS) is based on estimating the same parameter in two different ways: voltage model and current model. The speed estimation could be obtained using the rotor flux, back EMF, or reactive power. However, this technique may result in an amplification of the flux component estimation errors [3, 5, 6]. The closed loop observers such as the Luenberger observer are established from the dynamic model of the drive system and use measurements to estimate the rotor speed [10, 11]. In a stochastic environment, the extended Kalman filter (EKF) can be used to observe and predict the position and speed of the IM [13]. Several optimization methods have been developed to overcome the complex time of this observer using artificial intelligence [13, 14]. The sliding mode is known for its simplicity, easy implementation, robustness to parameter variation, and no extensive computation. However, the chattering phenomenon decreases its performance [6].

Considered as a nonlinear time-varying system, the IM is sensitive to operating conditions such as speed and mechanical load. Moreover, its parameters, in particular the rotor and stator resistances, vary with temperature, the electromagnetic state of the IM, and the frequency. These parameters significantly influence the estimation and control performance and variation in load torque. For this reason, the adaptation of parameters attracts more interest, especially when doing so influences not only the speed error but also stability in the drive system[5].

Several methods of stator resistance online estimation are presented in the literature. Among these, a full order sliding mode is developed [15] to estimate the rotor speed and the stator resistance by replacing a sign function with a sigmoid function to reduce the chattering phenomenon. In Khan and Verna [16], a P_n MRAS-based resistance estimator is proposed. The estimation is based on the error between the reference model output and the adjustable model output $(P_n^* - P_n)$ followed by a PI controller. Benlaloui et al. [17] present a PI MRAS adaptation law using two differences signals computed from the rotor fluxes and the electromagnetic torque estimation, while Krishna and Daya [18] developed a fuzzy-based stator resistance adaptation mechanism in the MRAS estimator.

In the present paper, a robust technique is presented for a sensorless vector control using a full-order observer to estimate the rotor flux and stator current. First, the rotor speed is estimated using the adaptive law, which verifies the stability criteria of the Lyapunov theorem. To overcome the sensitivity to parameter variations, the genetic algorithm program is used to estimate the stator resistance. Furthermore, the estimated speed and the current measurements are used to determine the load torque to improve the accuracy of the response of the system drive. In the simulation results, a comparison is given to show the influence of the developed adaptation mechanism.

Therefore, the manuscript is structured as follows. First, the modeling of the motor and the rotor field orientated control (RFOC) is presented. Then we describe in detail the design of the full order observer and the synthesis of the rotor speed estimation and the stator resistance adaptation mechanism.

2. Dynamic model of the induction motor and vector control

2.1. Dynamic model

Based on the equations describing the electromagnetic behavior, the dynamic model of the IM can be presented by the following equations expressed in the d-q reference frame [6]:

$$
\begin{cases}
\frac{dI_{ds}}{dt} = \lambda I_{ds} + \omega_s I_{qs} + \frac{M}{\sigma L_s L_r \tau_r}\Phi_{dr} + \frac{M}{\sigma L_s L_r}\omega\Phi_{qr} + \frac{1}{\sigma L_s}V_{ds} \\
\frac{dI_{qs}}{dt} = -\omega_s I_{ds} + \lambda I_{qs} - \frac{M}{\sigma L_s L_r}\omega\Phi_{dr} + \frac{M}{\sigma L_s L_r \tau_r}\Phi_{qr} + \frac{1}{\sigma L_s}V_{ds} \\
\frac{d\Phi_{dr}}{dt} = \frac{M}{\tau_r}I_{ds} - \frac{1}{\tau_r}\Phi_{dr} + \omega_r\Phi_{qr} \\
\frac{d\Phi_{qr}}{dt} = \frac{M}{\tau_r}I_{qs} - \omega_r\Phi_{dr} - \frac{1}{\tau_r}\Phi_{qr} \\
\frac{d\Omega}{dt} = \frac{pM}{L_r J}(\Phi_{dr}I_{qs} - \Phi_{qr}I_{ds}) - \frac{1}{J}T_l - \frac{f}{J}\Omega,
\end{cases}
\tag{1}
$$

where $\lambda = -(\frac{1}{\sigma\tau_s} + \frac{1-\sigma}{\sigma\tau_r})$.

2.2. Vector control

The vector control is based on the orientation of the flux in some way to imitate the DC motor behavior. This operation allows separate control of the flux and the torque by adjusting respectively the direct and quadrature components of the stator current. This technique is based on orientation of the dq reference so as to eliminate the quadrature component. Thus, for the RFOC the quadrature component of the flux is considered zero $\phi_{qr} = 0$, and so the flux will be carried entirely on the direct component $\phi_r = \phi_{dr}$. As a result, the control law

can be given by the following equations:

$$I_{ds} = \frac{1 + \tau_r s}{M}\Phi_r \tag{2}$$

$$I_{qs} = \frac{L_r}{pM}T_e \tag{3}$$

$$\omega_r = \frac{M}{\tau_r \Phi_r}I_{qs} \tag{4}$$

To obtain improved flux response, a flux regulator can be employed; it is called direct vector control. When this regulator is used, parameter sensitivity is less than that in indirect control. In addition, to obtain improved response and less sensitivity to machine parameters, a variety of flux observers can be used [19].

The general structure of the control is based on three main loops in a cascade topology. In addition to the flux loop, the torque loop is the inner one and it receives its command from the speed loop controller shown in Figure 2. The electromagnetic torque is the output of the IP controller in the speed loop.
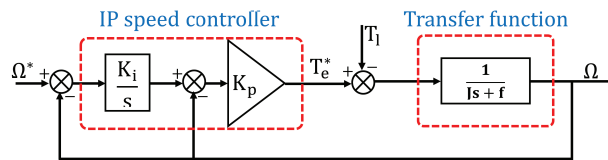

Figure 2. IP speed controller.

Note that the IP controller is chosen due to the absence of zero in the closed loop transfer function [19]. In absence of disturbances, the load torque is considered zero, and the closed-loop transfer function is given by

$$\frac{\hat{\Omega}}{\Omega^*} = \frac{1}{\frac{1}{K_p K_i}s^2 + \frac{f+K_p}{K_p K_i}s + 1} = \frac{1}{\frac{1}{\omega_0^2}s^2 + \frac{2\xi}{\omega_0}s + 1}, \tag{5}$$

where $\hat{\Omega}$ is the estimated speed given by the full-order Luenberger observer explained later in the next paragraph. By setting the desired response time, the controller gains are calculated by resolving the system:

$$\begin{cases} \frac{1}{\omega_0^2} = \frac{1}{K_p K_i} \\ \frac{2\xi}{\omega_0} = \frac{f+K_p}{K_p K_i} \end{cases}, \tag{6}$$

where ω_0 is the natural frequency and ξ the damping ratio.

To improve the response, the load torque is estimated from the measured stator current and estimated speed and flux from the system:

$$\begin{cases} \frac{d\hat{\Omega}}{dt} = -\frac{f}{J}\hat{\Omega} - \frac{\hat{T}_l}{J} + \frac{pM\Phi_r}{JL_r}I_{sq} \\ \frac{d\hat{T}_l}{dt} = 0 \end{cases} \tag{7}$$

3. Design of the full-order Luenberger observer for rotor speed estimation and stator resistance adaptation

3.1. Design of the observer

The full-order observer is based on the dynamic model of the IM in the stationary reference frame $\alpha\beta$ to avoid extra calculations and nonlinear transformations. The principle is to add a correction term to a copy of the system dynamics. The state representation is given by

$$\begin{cases} \dot{\hat{x}} & = & A x + B u + L(y - \hat{y}) \\ \hat{y} & = & C\hat{x} \end{cases} \tag{8}$$

As the stator current measurements and the rotor flux equations are easy to explore, the state vector is composed as follows: $x = \begin{pmatrix} \underline{I_s} \\ \underline{\Phi_r} \end{pmatrix}$.

Then the state matrix: $\begin{pmatrix} A_{11} & A_{12} \\ A_{21} & A_{22} \end{pmatrix} = \begin{pmatrix} a_{11}^i I & a_{12}^i I + a_{12}^j J \\ a_{21}^i I & a_{22}^i I + a_{22}^j J \end{pmatrix}$

$$a_{11}^i = \lambda \qquad a_{12}^i = \frac{M}{\sigma L_s L_r \tau_r} \qquad a_{12}^j = \frac{M}{\sigma L_s L_r}\omega \qquad a_{21}^i = \frac{M}{\tau_r} \qquad a_{22}^i = \frac{-1}{\tau_r} \qquad a_{22}^j = \omega$$

The input and the output vectors: $u = \underline{V_s}$ $\qquad y = \underline{I_s}$

The input and the output matrix: $B = \frac{1}{\sigma L_s}I$ $\qquad C = \begin{pmatrix} 1 & 0 \end{pmatrix}$

Luenberger gain matrix: $L = \begin{pmatrix} L_1 \\ L_2 \end{pmatrix} = \begin{pmatrix} l_{11}I + l_{12}J \\ l_{21}I + l_{22}J \end{pmatrix}$

The main objective is to determine the gain matrix L, which will be explained in the following paragraph.

3.2. Proof of stability observer

The observer's dynamic is set by the choice of the gain matrix that significantly affects the poles of the system. These poles are the eigenvalues of the matrix $A - LC$. They must be chosen so as to ensure the stability of the observer.

The eigenvalues of the induction motor λ_{IM} are given by solving the following characteristic polynomial:

$$det(\lambda_{IM}I - A) = \lambda_{IM}^2 - (A_{11} + A_{22})\lambda_{IM} - A_{12}A_{21} + A_{11}A_{22} = 0 \tag{9}$$

The eigenvalues of the Luenberger observer λ_{LO} are given by

$$det(\lambda_{LO}I - A + LC) = \lambda_{LO}^2 - (A_{11} + A_{22} - L_1)\lambda_{LO} - A_{12}A_{21} + A_{11}A_{22} - A_{22}L_1 + A_{12}L_2 = 0 \tag{10}$$

For stability reasons and system dynamics, the eigenvalues of the observer must be chosen proportional to those of the IM according to the equation $\lambda_{LO} = K\lambda_{IM}$ $(K > 1)$ [20]. By replacing this equation in (10) and by identification with K^2 (9) we obtain the following gain matrix:

$$\begin{cases} L_1 & = & -(K-1)((a_{11}^i + a_{22}^i)I - a_{22}^j J) \\ L_2 & = & (K-1)[((a_{11}^i + a_{22}^i) - \frac{(K+1)(a_{12}^i a_{21}^i + a_{11}^i a_{22}^i)}{a_{12}^i})I + (\frac{a_{11}^i a_{22}^i a_{22}^j - a_{22}^{j2}}{a_{12}^j} - \frac{(K+1)(a_{12}^j a_{21}^i + a_{11}^i a_{22}^j)}{a_{12}^j})J] \end{cases} \tag{11}$$

As can be seen in Figure 3, the trajectory of the full-order observer pole depends on the choice of the appropriate value of the gain matrix. Indeed, the choice of the gain matrix defines not only the dynamics of the observer but also its stability. As shown in Figure 4, when K increases the system tends to lose its stability.
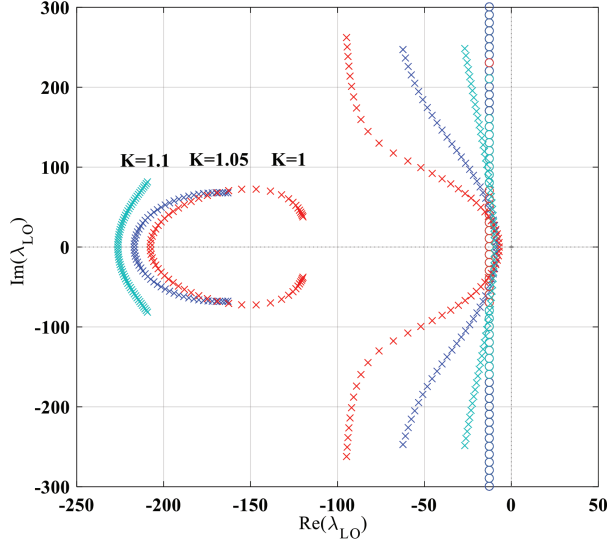

Figure 3. Trajectory of the full-order Luenberger observer pole for different speeds.
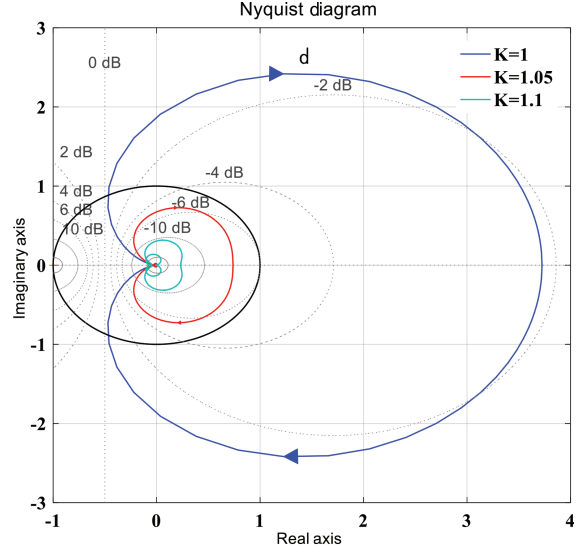
Figure 4. Nyquist diagram of the Luenberger observer for different values of K.

3.3. Rotor speed adaptation

To ensure observer stability, we use the Lyapunov criterion. Then the candidate function chosen for estimating the rotor speed is given by [20]

$$V_\omega = e^T e + \frac{\Delta\omega^2}{\tau_\omega}, \tag{12}$$

where $e = x - \hat{x}$ and $\dot{e} = \hat{A}e + \Delta A\hat{x}$ are the estimation error and its derivative, respectively.

$\Delta A = A(\omega) - A(\hat{\omega})$ defines the difference between the state matrix for the real and estimated speed. Therefore, the derivative function of V_ω is given by

$$\frac{dV_\omega}{dt} = e^T(\hat{A}^T + \hat{A})e + 2a_{12}^i\tau_r(\hat{\Phi}_{r\beta}e_{I_{s\alpha}} - \hat{\Phi}_{r\alpha}e_{I_{s\beta}})\Delta\omega - 2(\hat{\Phi}_{r\alpha}e_{\Phi_{r\alpha}} - \hat{\Phi}_{r\beta}e_{\Phi r\beta})\Delta\omega - 2\frac{\Delta\omega}{\tau_\omega}\frac{d\hat{\omega}}{dt} \tag{13}$$

To satisfy the Lyapunov criterion, the estimated speed must be defined as a pure integration in the open loop of the cross product of estimated flux and the current error:

$$\hat{\omega} = \frac{a_{12}^i\tau_r}{\tau_\omega}\int(\hat{\Phi}_{r\beta}e_{I_{s\alpha}} - \hat{\Phi}_{r\alpha}e_{I_{s\beta}}) \tag{14}$$

To improve the estimation speed, a PI adaptation mechanism is proposed.

3.4. Parameter adaptation using the GA-based mechanism

As mentioned before, the vector control is sensitive to the IM parameters, especially the stator resistance. For this reason an adaptation mechanism should be established. The proof of stability is based on the Lyapunov theorem as done before for the rotor speed. Then the candidate function and its derivative are given by

$$V = V_\omega + \frac{\Delta R_s^2}{\tau_{R_s}} \qquad \Longrightarrow \qquad \frac{dV}{dt} = \frac{dV_\omega}{dt} - \frac{2}{\sigma}(\hat{I}_{s\alpha}e_{I_{s\alpha}} + \hat{I}_{s\beta}e_{I_{s\beta}})\Delta R_s - 2\frac{\Delta R_s}{\tau_{R_s}}\frac{d\hat{R}_s}{dt} \qquad (15)$$

Thus, we obtain the following adaptation mechanism of the stator resistance estimation:

$$\hat{R}_s = (K_p + \frac{K_i}{s})(\hat{I}_{s\alpha}e_{I_{s\alpha}} + \hat{I}_{s\beta}e_{I_{s\beta}}) \qquad (16)$$

The problem occurring at this level is the determination of the controller gain. Indeed, there is no algebraic method; only the error test technique is used. To overcome this random determination of these parameters, genetic algorithm optimization is used. The purpose is to consider the adaptation law obtained by the Lyapunov criterion as a minimization problem. Indeed, the fitness function (the input argument to the main GA program) is defined by Equation (16).

The genetic algorithm is based on natural selection. It is a method for solving optimization problems. This technique is built on repeated modification of the population in such a way as to evolve toward an optimal solution [21]. In this vein, to create the next generation from the current population at each step, the genetic algorithm uses three main rules: selection, crossover, and mutation. The diagram shown in Figure 5 summarizes the different steps of the GA optimization. The control optimization used is shown in Figure 6 and the parameters of the GA-based program are summarized in Table 1.

Table 1. GA parameters.

Property	Value
Number of values	2
Population size	50
Maximum number of generation	100
Mutation fraction	0.1
Crossover fraction	0.8
Tolerance	10^{-6}

To summarize, the structure of the improved sensorless vector control is shown in Figure 7. A full-order Luenberger observer is used to estimate the rotor flux and the stator currents followed by a PI adaptation mechanism to estimate the rotor speed. For the stator resistance estimation, GA-based control optimization is applied. To improve the accuracy of the response of the system, the load torque is restored.

4. Simulation results

The Simulink model used to verify the proposed structure is presented in Figure 8. The IM parameters are shown in Table 2.

The following simulations are carried for many ranges of speed while the motor is loaded. As shown in Figure 9a, the speed at the beginning is zero; then it gradually increases in ramp. The speed is kept constant
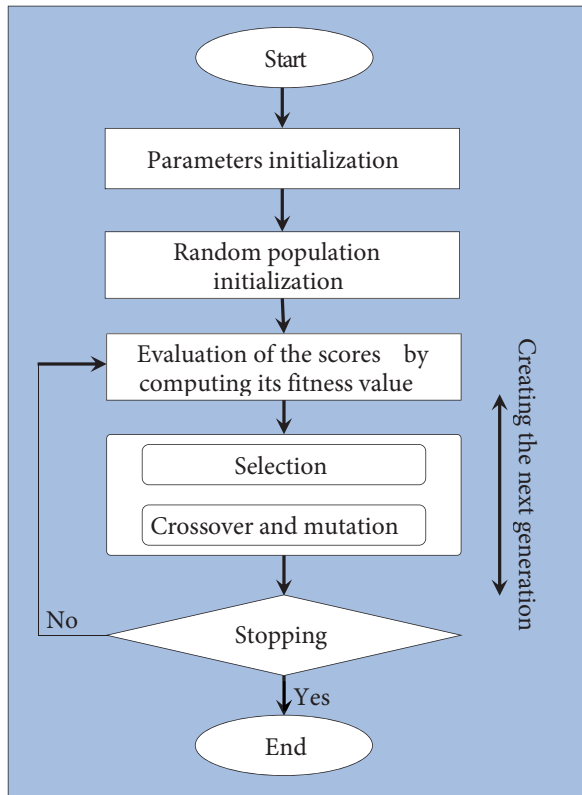
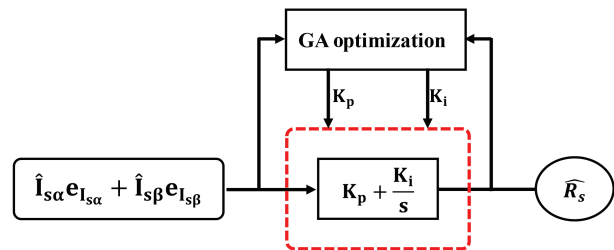Figure 5. GA optimization diagram.

Figure 6. GA-based control optimization.

Table 2. Induction motor specifications and parameters.

Technical specifications			Parameters		
Rated power	160	KW	R_s, R_r	0.01379, 0.007728	Ω
Rated voltage	400	V	L_s, L_r	0.0078, 0.0078	H
Rated frequency	50	Hz	Mutual inductance	0.00769	H
Rated speed	1487	rpm	Total inertia	2.9	$Kg.m^2$
Number of pole pairs	2		Friction coefficient	0.05658	$Nm.s.rad^-1$

every 2 s (100 rpm, 700 rpm, then to 1500 rpm). The stator resistance variation is applied at 3 s. It is increased by 50% of the rated value. At 12 s, the stator resistance is set to its rated value.

The abrupt increase in stator resistance influences the response of the system. However, the GA-based adaptation reduces this effect as can be noted in the simulation results. Indeed, when using the GA-based adaptation, the stator variation generates a small oscillation for the speed (Figures 9a and 9b), a peak for the electromagnetic torque (Figures 9c and 9d) and a slight variation in the flux (Figure 10).

Without adaptation, the orientation of the flux is no longer maintained (Figure 10). The absence of the adaptation mechanism generates divergence of the measured current of its reference and then divergence of the electromagnetic torque. As mentioned before, the q-axis stator current is proportional to the electromagnetic torque by Equation (2). This can be noted in Figure 9c and Figures 11a and 11b. Moreover, a distortion
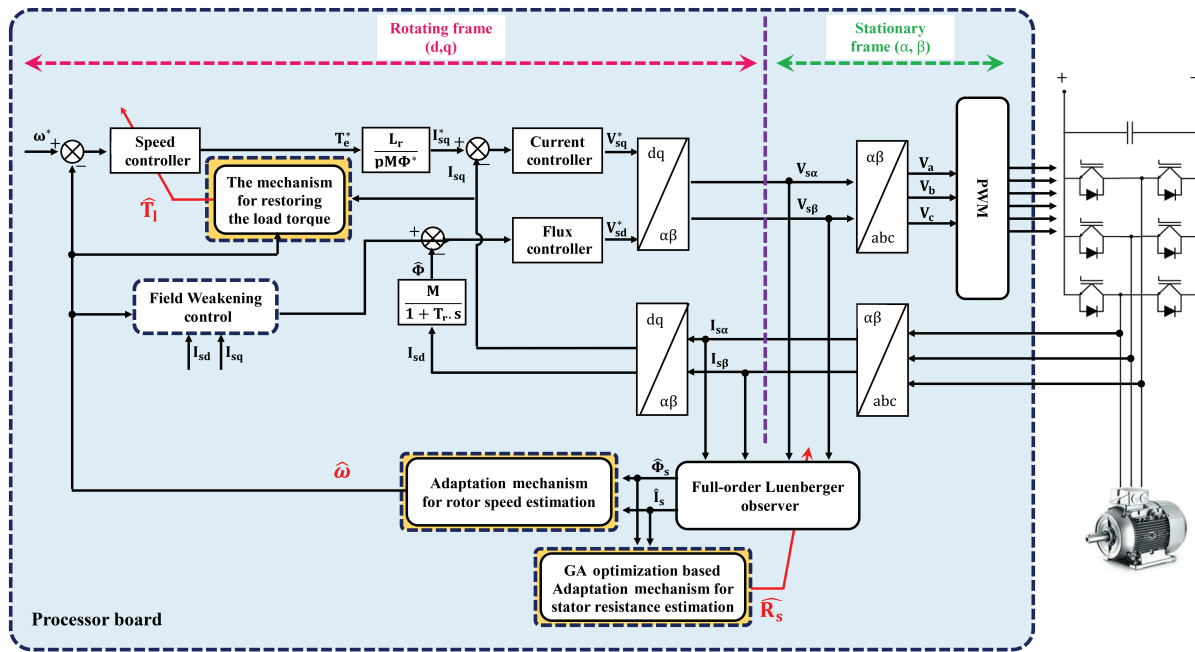
Figure 7. Block diagram of sensorless vector control using a Luenberger observer for rotor speed estimation with online load torque estimation and stator resistance adaptation.
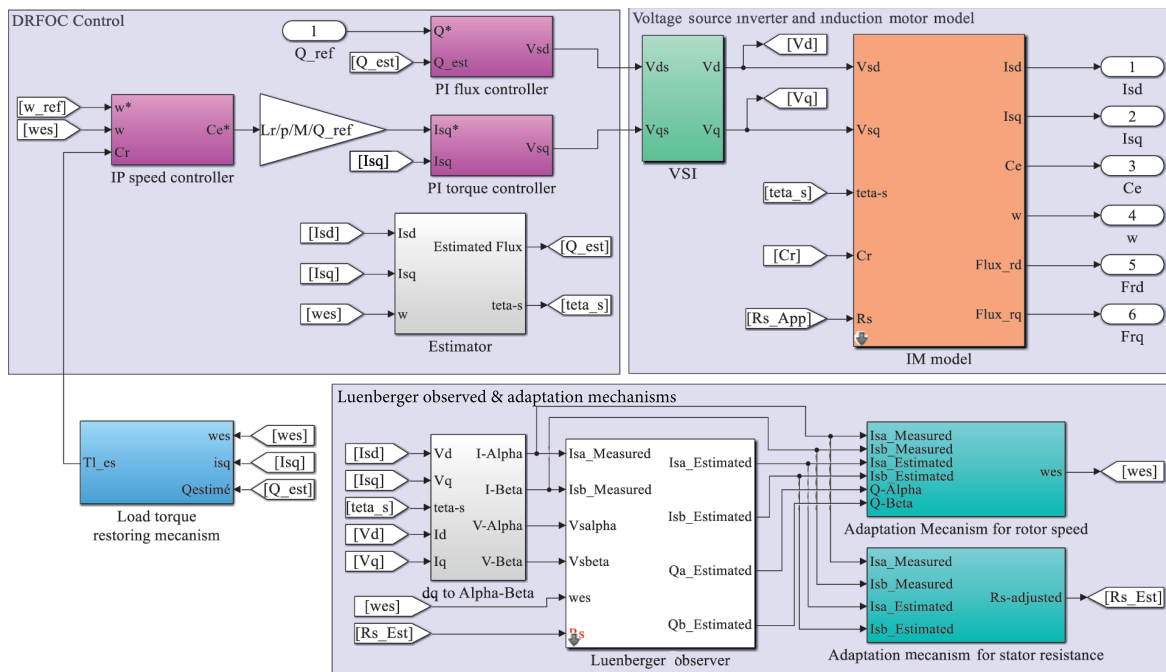

Figure 8. Simulink model of the proposed structure.

of the three-phase current appears in the absence of adaptation (Figure 11c). By comparing the applied and the estimated resistance (Figure 11d), we can observe that the estimated resistance follows its reference. Furthermore, this estimation is sensitive to the speed variation.
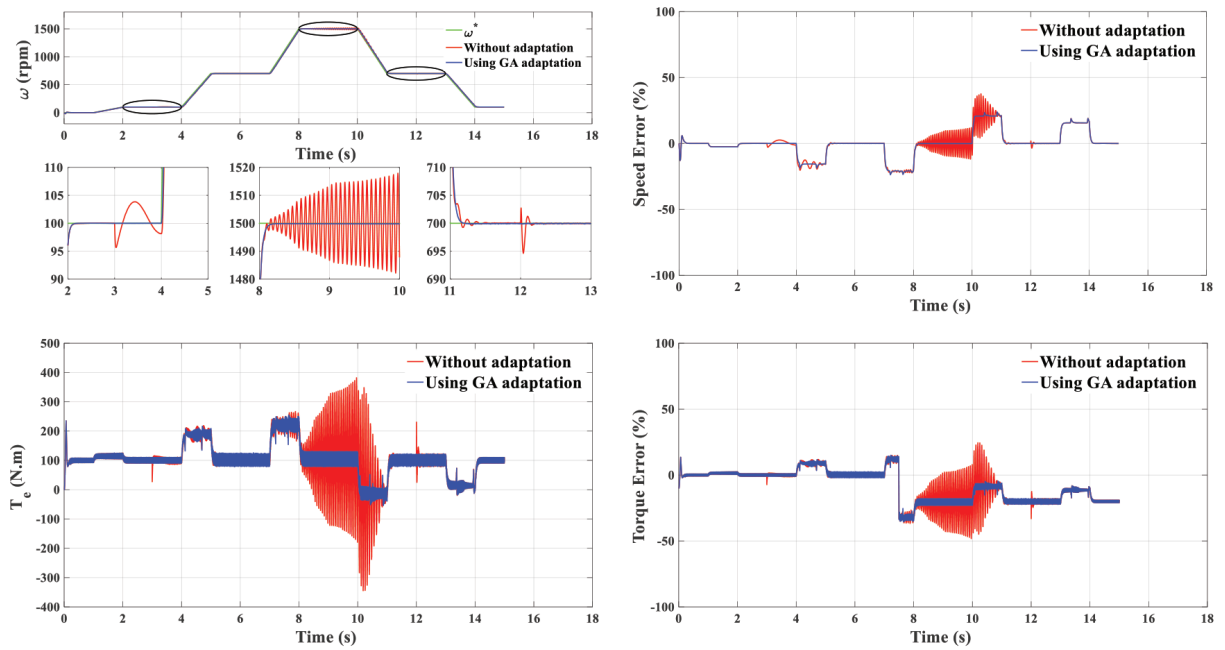
Figure 9. (a) Speed response, (b) speed error (%), (c) electromagnetic torque response, (d) torque error (%) (at rated torque).
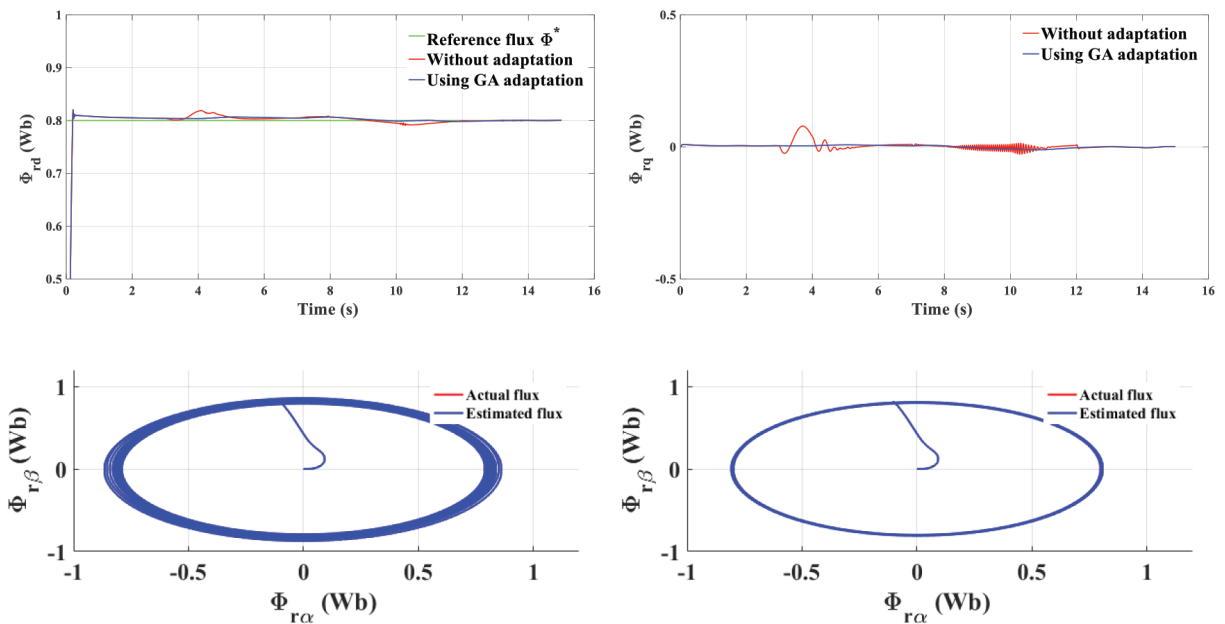

Figure 10. (a) d-axis rotor flux response, (b) q-axis rotor flux response, (c) rotor flux in the stationary frame without adaptation, (d) rotor flux in the stationary frame using GA-based adaptation (at rated torque).

To verify the proposed structure for reversal speeds, we gradually apply a slew rate ramp speed from 0 to 1000 rpm and this is kept constant for 6 s and then reversed in ramp to –1000 rpm and maintained constant for 7 s. In addition, the rated load torque of the IM drive is applied during the first 7 s and then inverted for
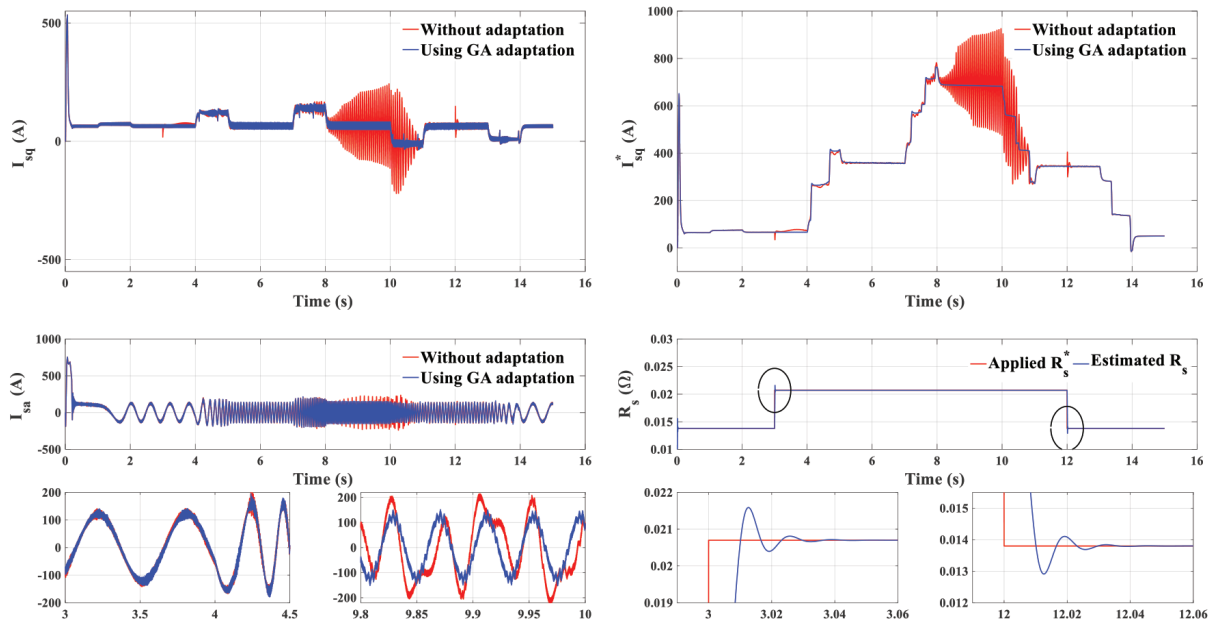
Figure 11. (a) q-axis measured stator current, (b) q-axis reference stator current, (c) one-phase stator current, (d) stator resistance estimation (at rated torque).

the last 7 s so that the IM always works in motor mode. A 70% variation in the stator resistance is applied at 3 s and removed at 12 s. Figure 12a shows the speed response and Figure 12b its error. Speed ripples appear at 3 s and 12 s due to the variation in stator resistance. It can also be seen in the torque response and its error as shown respectively in Figures 12c and 12d. The flux orientation is no longer assured without the adaptation mechanism (Figure 13).

The speed passes through zero when it is inverted, which causes a divergence in the velocity error. This error is canceled more quickly when the adaptation is used (Figure 12b).

The q-axis stator current is presented in Figures 14a and 14b, the three-phase stator current in Figure 14c, and the applied and estimated stator resistance in Figure 14d.

The present study emphasizes only the adaptation of the stator resistance due to the high sensitivity of control to this parameter compared to the rotor resistance, which explains the choice of the proposed adaptation. Indeed, a 50% variation in the stator resistance causes ripples of speed around its final value (Figure 15a) and a nonnegligible error of torque (Figure 15b) and the flux orientation is no longer maintained (Figures 15c and 15d). For higher values, this can lead to system instability. However, the effect of variation in rotor resistance as shown in Figure 15b is negligible and the system remains stable even with +50% rotor resistance variation.

According to the simulations carried out, the high sensitivity to stator resistance variations at low and rated speed can be deduced. Indeed, the rotor speed is directly affected by the flux estimation error due to the resistance variations. For higher values, the system becomes unstable without the parametric adaptation.

As shown in Figure 16, the GA-based controller determines the stator resistance even if the variation reaches higher values.

At the end of this section, the proposed structure is tested for different ranges of speed (low, medium, high, and reversal) under different conditions. The performance results obtained for the proposed control strategy
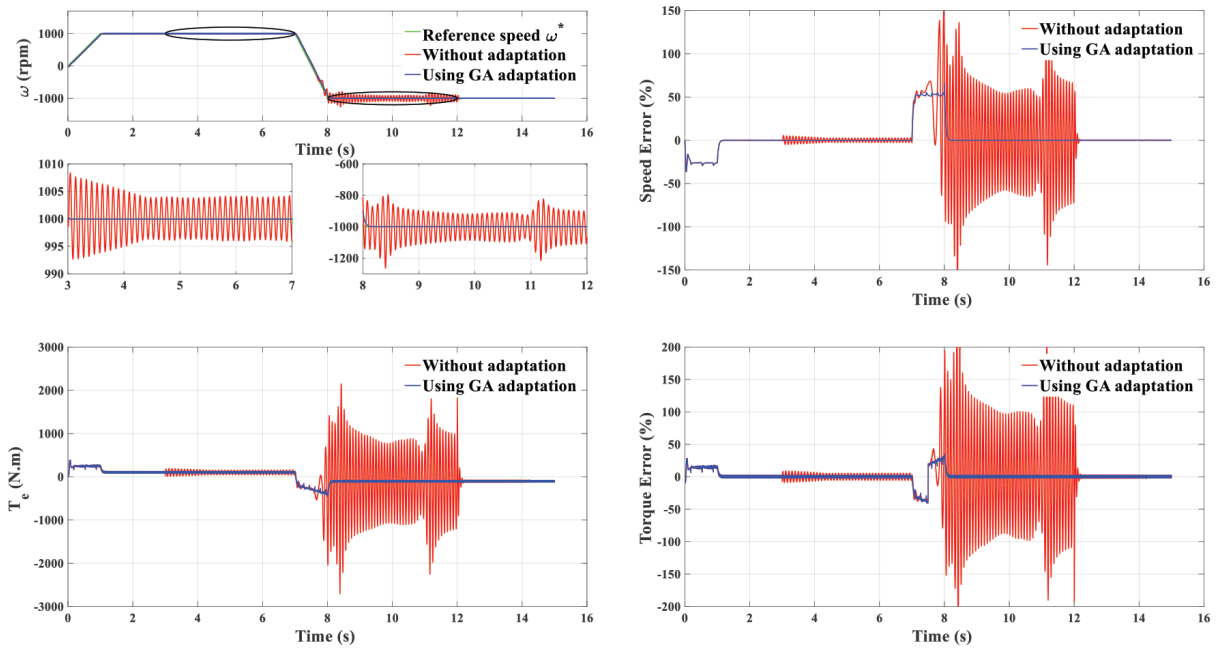
Figure 12. (a) Speed response, (b) speed error (%), (c) electromagnetic torque response, (d) torque error (%) (reversal speed).
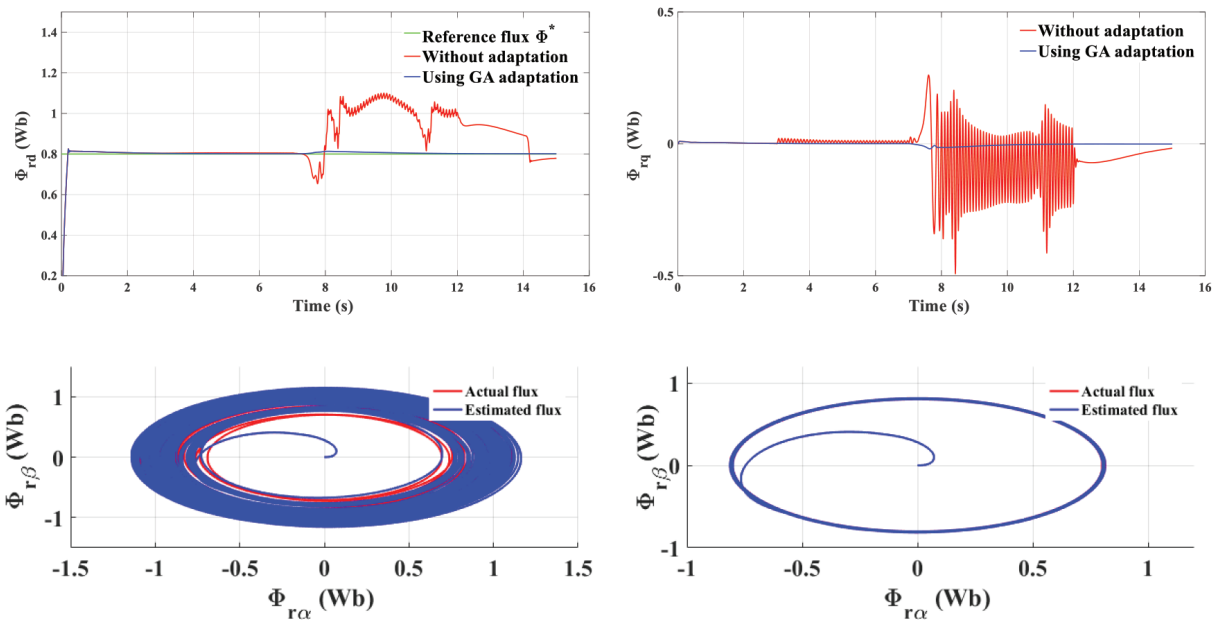

Figure 13. (a) d-axis rotor flux response, (b) q-axis rotor flux response, (c) rotor flux in the stationary frame without adaptation, (d) rotor flux in the stationary frame using GA-based adaptation (reversal speed).

present effectiveness, robustness, and stability. The present study has the peculiarity of using the GA-based control to determine the controller gains by considering the adaptive law as a minimization problem. Previous
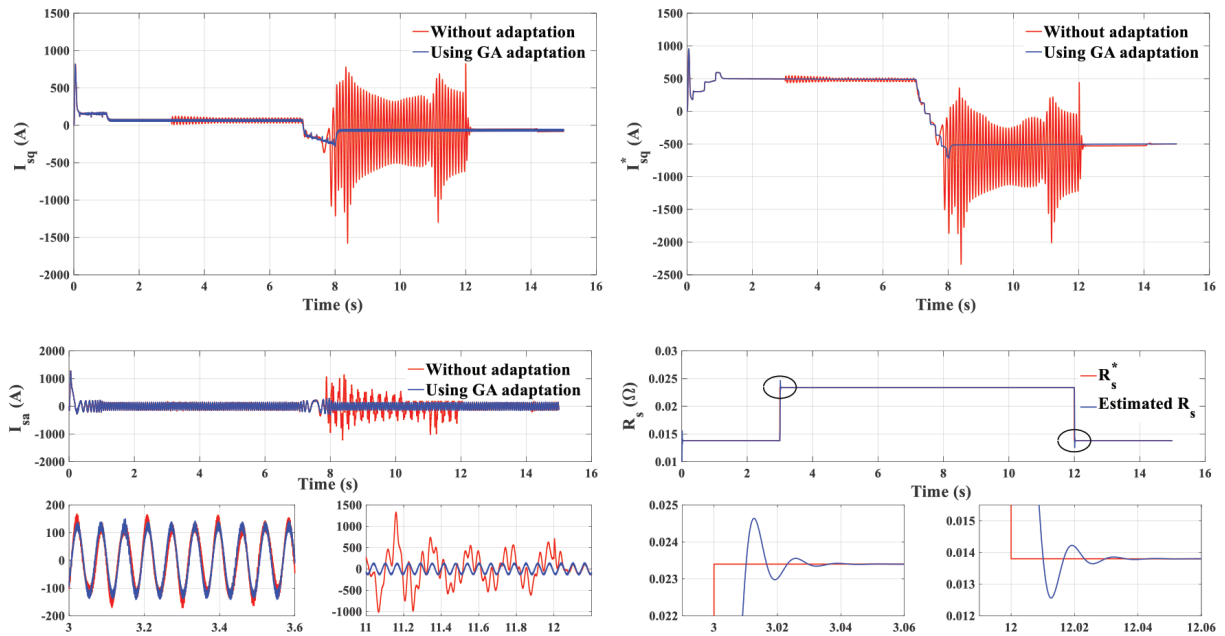
Figure 14. (a) q-axis measured stator current, (b) q-axis reference stator current, (c) one-phase stator current, (d) stator resistance estimation (reversal speed).
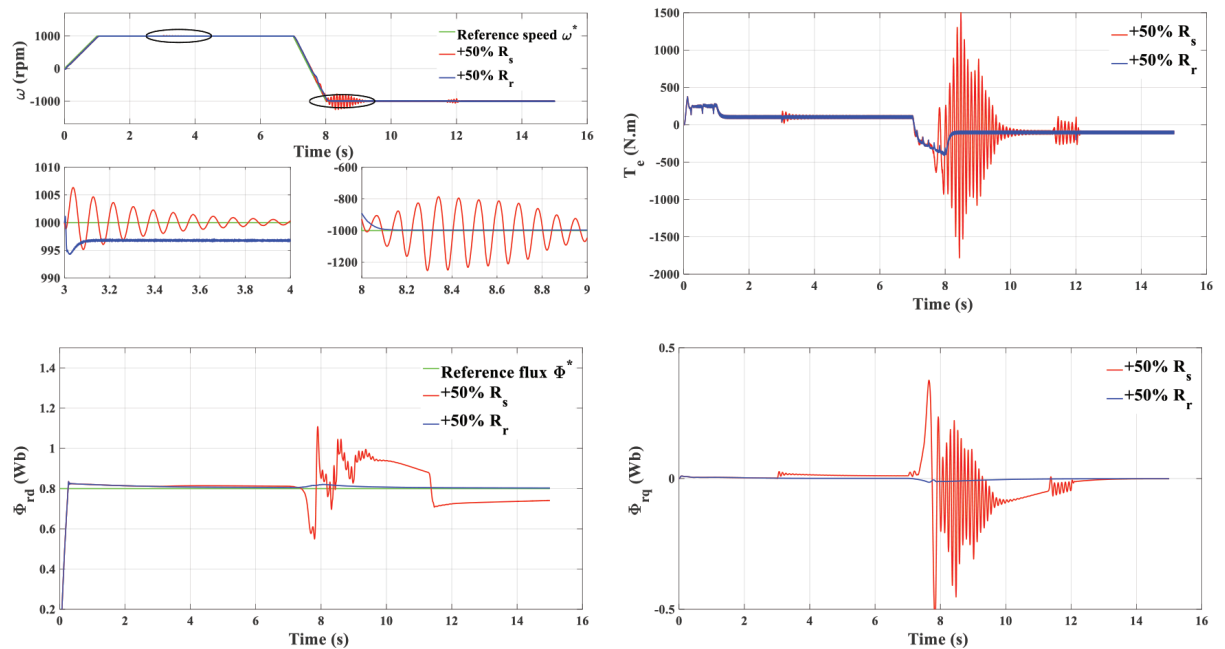
Figure 15. (a) Speed response, (b) electromagnetic torque response, (c) d-axis rotor flux, (d) q-axis rotor flux.

studies [6, 16, 17] mainly use a conventional PI controller or use a simple online compensator based on the error between measured and observed $\alpha\beta$ axis stator currents [15]. Others propose a robust method based on the multiobjective adaptive fuzzy Luenberger observer independently on rotor resistance variation [22]. The results
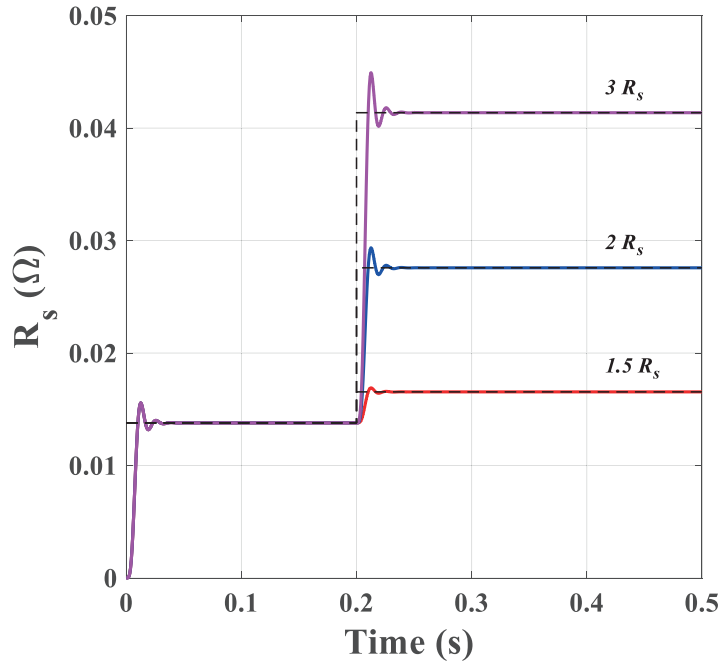
Figure 16. GA-based controller response for different applied stator resistance.

show the robustness of the control under rated torque and rotor resistance variation. However, the results did not take into account the stator resistance impact to validate the proposed structure. Furthermore, in [23], the feedback linearization based control is combined with an MRAS-SMO and applied to the sensorless direct torque control. The structure is verified under different conditions and shows effectiveness and stability. However, the parametric sensitivity is not verified.

5. Conclusion

In the present paper, an improved structure for sensorless control of IM drives is proposed. The full-order Luenberger observer is employed to estimate the rotor flux and stator currents used to define the adaptation law for the rotor speed based on the Lyapunov theorem. A GA-based adaptation is used to estimate the stator resistance. The purpose is to define an adaptive law as a minimization problem. This adaptive law constitutes the input of the GA optimization. Furthermore, and to improve the accuracy of the system response, the load torque is restored using the estimated speed and measured currents.

To validate this work, simulations are carried out for different ranges of speed and different environments (e.g., load torque applied, parameter variation). The comparison between the system response without the adaptation mechanism and with the GA-based control shows the main quality of the novel structure. Indeed, the simulation results allow us to obtain an improved response over the entire speed range, even in the zero zone and at low speed. This control allows for less sensitivity to machine parameters. In fact, the flux orientation is ensured in the presence of a parametric variation in stator resistance, and the system remains stable even if the variation reaches high values. This is well suited for urban electric vehicles. This engine, like many other

applications, is working in a difficult environment, and the priority is to maintain the system's stability through its optimum operation.

Nomenclature

$*$ and $\wedge$	:	Respectively denote the references and estimated values.
$R_{s,r}$	:	Stator and rotor resistances.
$L_{s,r}$ and M	:	Stator, rotor, and mutual inductances.
p, J, and f	:	Respectively pole pairs number, total inertia, and friction coefficient.
$V_{ds,qs}$, $V_{dr,qr}$	:	d-q stator and rotor voltages.
$I_{ds,qs}$, $I_{dr,qr}$	:	d-q stator and rotor currents.
$\Phi_{ds,qs}$, $\Phi_{dr,qr}$	:	d-q stator and rotor fluxes.
$\omega_{s,r}$	:	Synchronous and slip speed.
$\omega = p\Omega = \omega_s - \omega_r$	:	Electrical rotor speed.
Ω	:	Mechanical rotor speed.
T_e and T_l	:	Respectively electromagnetic torque and load torque.
$\tau_{s,r} = \frac{L_{s,r}}{R_{s,r}}$	:	Stator and rotor time constant.
$\sigma = 1 - \frac{M^2}{L_s L_r}$	:	Leakage coefficient.

References

[1] Saidur R, Mekhilef S, Ali MB, Safari A, Mohammed HA. Applications of variable speed drive (VSD) in electrical motors energy savings. Renewable and Sustainable Energy Reviews 2012; 16 (1): 543-50. doi: 10.1016/j.rser.2011.08.020

[2] Crowder R. Induction motors. In: Crowder R (editor). Electric Drives and Electromechanical Systems: Applications and Control. Burlington, MA, USA: Butterworth-Heinemann, 2019, pp. 191-214.

[3] Wang G, Yu Y, Zhang G, Wang B, Yang M et al. Sensorless control of motor drives. In: Blaabjerg F (editor). Control of Power Electronic Converters and Systems. USA: Academic Press, 2018, pp.331-369.

[4] Rind S, Ren Y, Jiang L. MRAS based speed sensorless indirect vector control of induction motor drive for electric vehicles. In: 2014 49th International Universities Power Engineering Conference; Cluj-Napoca, Romania; 2014. pp. 7-30. doi: 10.1109/UPEC.2014.6934645

[5] Alsofyani IM, Idris NR. A review on sensorless techniques for sustainable reliability and efficient variable frequency drives of induction motors. Renewable and Sustainable Energy Reviews 2013; 24: 111-121. doi: 10.1016/j.rser.2013.03.051

[6] Moutchou M, Abbou A, Mahmoudi H. MRAS-based sensorless speed backstepping control for induction machine, using a flux sliding mode observer. Turkish Journal of Electrical Engineering & Computer Sciences 2015; 23 (1): 187-200. doi: 10.3906/elk-1208-50

[7] Zidani Y, Zouggar S, Elbacha A. Steady-state analysis and voltage control of the self-excited induction generator using artificial neural network and an active filter. Iranian Journal of Science and Technology, Transactions of Electrical Engineering 2018; 42 (1): 41-48. doi: 10.1007/s40998-017-0046-0

[8] Bouhoune K, Yazid K, Boucherit MS, Cheriti A. Hybrid control of the three phase induction machine using artificial neural networks and fuzzy logic. Applied Soft Computing 2017; 55: 289-301. doi: 10.1016/j.asoc.2017.01.048

[9] Bahloul M, Souissi M, Chaabane M, Alaoui LC, Drid S. Fuzzy speed estimation in the case of sensorless induction machine vector control. Turkish Journal of Electrical Engineering & Computer Science 2016; 24 (5): 3961-3975. doi: 10.3906/elk-1412-82

[10] Jouili M, Jarray K, Koubaa Y, Boussak M. Luenberger state observer for speed sensorless ISFOC induction motor drives. Electric Power Systems Research 2012; 89: 139-147. doi: 10.1016/j.epsr.2012.02.014

[11] Aydeniz MG, Şenol İ. A Luenberger-sliding mode observer with rotor time constant parameter estimation in induction motor drives. Turkish Journal of Electrical Engineering & Computer Sciences 2011; 19 (6): 901-912. doi: 10.3906/elk-1004-4

[12] Zerdali E, Barut M. Novel version of bi input-extended Kalman filter for speed-sensorless control of induction motors with estimations of rotor and stator resistances, load torque, and inertia. Turkish Journal of Electrical Engineering & Computer Sciences 2016; 24 (5): 4525-4544. doi: 10.3906/elk-1408-136

[13] Barut M, Demir R, Zerdali E, Inan R. Real-time implementation of bi input-extended Kalman filter-based estimator for speed-sensorless control of induction motors. IEEE Transactions on Industrial Electronics 2011; 59 (11): 4197-4206. doi: 10.1109/TIE.2011.2178209

[14] Alsofyani IM, Idris NR, Sutikno T, Alamri YA. An optimized extended Kalman filter for speed sensorless direct troque control of an induction motor. In: 2012 IEEE International Conference on Power and Energy; 2012. pp. 319-324. doi: 10.1109/PECon.2012.6450230

[15] Saadaoui O, Khlaief A, Abassi M, Tlili I, Chaari A et al. A new full-order sliding mode observer based rotor speed and stator resistance estimation for sensorless vector controlled PMSM drives. Asian Journal of Control 2019; 21 (3): 1318-1327. doi: 10.1002/asjc.1812

[16] Khan YA, Verma V. A novel method of estimating stator resistance for an F-MRAS based speed sensorless vector controlled switched reluctance motor drive. In: 2019 54th International Universities Power Engineering Conference; Bucharest, Romania; 2019. pp. 1-6. doi: 10.1109/UPEC.2019.8893490

[17] Benlaloui I, Drid S, Chrifi-Alaoui L, Ouriagli M. Implementation of a new MRAS speed sensorless vector control of induction machine. IEEE Transactions on Energy Conversion 2014; 30 (2): 588-595. doi: 10.1109/TEC.2014.2366473

[18] Krishna SM, Daya JF. MRAS speed estimator with fuzzy and PI stator resistance adaptation for sensorless induction motor drives using RT-lab. Perspectives in Science 2016; 8: 121-126. doi: 10.1016/j.pisc.2016.04.013

[19] Lokriti A, Salhi I, Doubabi S, Zidani Y. Induction motor speed drive improvement using fuzzy IP-self-tuning controller. A real time implementation. ISA Transactions 2013; 52 (3): 406-417. doi: 10.1016/j.isatra.2012.11.002

[20] Kubota H, Matsuse K, Nakano T. DSP-based speed adaptive flux observer of induction motor. IEEE Transactions on Industry Applications 1993; 29 (2): 344-348. doi: 10.1109/28.216542

[21] Aydoğdu Ö, Akkaya R. An effective real coded GA based fuzzy controller for speed control of a BLDC motor without speed sensor. Turkish Journal of Electrical Engineering & Computer Sciences 2011; 19 (3): 413-430. doi: 10.3906/elk-0907-122

[22] Bahloul M, Chrifi-Alaoui L, Drid S, Souissi M, Chaabane M. Robust sensorless vector control of an induction machine using multiobjective adaptive fuzzy Luenberger observer. ISA Transactions 2018; 74: 144-154. doi: 10.1016/j.isatra.2018.01.019

[23] Ammar A, Kheldoun A, Metidji B, Ameid T, Azzoug Y. Feedback linearization based sensorless direct torque control using stator flux MRAS-sliding mode observer for induction motor drive. ISA Transactions 2020; 98: 382-392. doi: 10.1016/j.isatra.2019.08.061